Generating highly squeezed hybrid Laguerre-Gauss modes in large-Fresnel-number degenerate optical parametric oscillators

Carlos Navarrete-Benlloch, Germán J. de Valcárcel, and Eugenio Roldán
Departament d'Òptica, Universitat de València, Dr. Moliner 50, 46100 Burjassot, Spain
(Received 6 October 2008; published 21 April 2009)

We theoretically describe the quantum properties of a large-Fresnel-number degenerate optical parametric oscillator (DOPO) with spherical mirrors that is pumped by a Gaussian beam and is tuned at the subharmonic frequency to a given transverse-mode family. We first analyze the classical problem and find that only the Laguerre-Gauss modes with lowest orbital angular momentum (OAM) are amplified above threshold. The transverse symmetry of the classically emitted signal field depends on the family index f. If f is even the lowest available OAM is zero and emission occurs in a radially symmetric mode; on the contrary, if f is odd the lowest available OAM is 1 and the emitted signal field has the shape of a hybrid Laguerre-Gauss mode (a linear combination of the two Laguerre-Gauss modes with OAM equal to ± 1) that breaks the rotational invariance of the system. Next we focus on the squeezing properties of this DOPO model. As for the modes with lowest OAM we demonstrate that their quantum properties (in the linear approximation) are equal to the standard single-mode DOPO (for even f) or to the recently analyzed DOPO tuned to its first transverse-mode family [C. Navarrete-Benlloch, E. Roldán, and G. J. de Valcárcel, Phys. Rev. Lett. **100**, 203601 (2008)]. Concerning the rest of (classically empty) modes (having larger OAM) we find that combinations of Laguerre-Gauss modes with opposite OAM (hybrid Laguerre-Gauss modes) exhibit quadrature squeezing. This property is independent of the even or odd character of the family index and hence has nothing to do with the symmetry of the classically emitted signal field. Noticeably the amount of squeezing does not depend on the pump level (it is thus noncritical squeezing) and can be arbitrarily large for the lower OAM nonamplified modes.

DOI: 10.1103/PhysRevA.79.043820 PACS number(s): 42.50.Tx, 42.65.Yj, 42.50.Dv, 42.50.Lc

I. INTRODUCTION

Degenerate optical parametric oscillators (DOPOs) are nowadays the standard squeezed light source. Let us remind that a light mode is said to be squeezed if the fluctuations in one of its quadratures are below the standard quantum limit, which is defined as the vacuum fluctuations level of that quadrature [1–3]. In DOPOs, squeezing is accomplished; thanks to the parametric down-conversion process occurring in the nonlinear crystal together with the interference between the intracavity field and the external vacuum fluctuations that enter into the cavity through the output mirror [4]. Quantum noise reductions as large as 10 dB (90%) have been experimentally demonstrated with DOPOs [5].

High-precision measurements are perhaps the best known applications of squeezed light [3], but applications to quantum information with continuous variables are becoming increasingly important [6], as squeezed light is the essential ingredient in generating continuous-variable entanglement. Improving the quality and reliability of squeezing is thus an important goal, but the generation of squeezed light with particular spatial distributions could also be important. This has been shown to be of utility in, e.g., high-precision positioning [7]. Recently Laguerre-Gauss beams are attracting much attention because of the many potential applications of the orbital angular momentum (OAM) carried by these light beams [8], and the generation of nonclassical Laguerre-Gauss modes could thus lead to new phenomena in the interaction between these light fields and matter.

Here we consider squeezing generation by means of DOPOs with large-Fresnel-number cavities composed of spherical mirrors. In such systems, the cavity can sustain the nonlinear interaction for several transverse modes (diffraction losses are ideally suppressed) giving rise to new results concerning squeezing. Quantum fluctuations in large-Fresnel-number cavities have been studied in the past, and new phenomena resulting from the interplay between quantum fluctuations and transverse pattern formation have been predicted. Concerning cavities composed of planar mirrors, the phenomena of quantum images [9] (below threshold) and the perfect noncritical squeezing of the emerging transverse pattern linear momentum [10,11] (above threshold) have been predicted. Regarding spherical mirrors, only below threshold operation has been studied [12], showing that also in this case there appear quantum images anticipating the above threshold pattern.

Here we consider a DOPO cavity with spherical mirrors that is pumped by a Gaussian mode. The difference of our work with respect to previous analyses of large-Fresnel-number DOPOs consists in that we study the system above its oscillation threshold, while previous works have treated the below threshold case [9,12]. This has led us to quantum fluctuations phenomena that have not been previously described. Specifically, we shall assume that the DOPO cavity is exactly tuned to a particular family of Laguerre-Gauss transverse modes labeled by an integer f (consisting of $f+1$ frequency-degenerate Laguerre-Gauss modes with OAMs $\pm f, \pm(f-2), \ldots, \pm l_0$ with $l_0=0$ or 1 for even or odd f, respectively; this is reviewed in Appendix A). After deriving in Sec. II the system's model, we first demonstrate (Sec. III) that the DOPO above threshold emits a signal field consisting of pairs of photons with opposite OAM, $+l_0$ and $-l_0$; i.e., the DOPO emits in the transverse mode with the lower possible OAM, a result not derived previously. The squeez-

ing properties of this mode turn out to coincide with those derived in the past, as the case $l_0=0$ is equivalent to the standard DOPO model [2], and the case $l_0=1$ generalizes what has recently been described in [13,14]. After reviewing the squeezing properties of cases $f_0=0$ and 1 in Sec. IV A, we concentrate on the squeezing properties of the rest of modes (those with $l>l_0$ that remain off when the DOPO is above threshold) in Sec. IV B. In Sec. IV C we will demonstrate the main result of the present work, namely, that certain combinations of opposite OAM modes exhibit large squeezing (which is larger for the larger values of f and the lower values of l). Remarkably, this squeezing is noncritical, i.e., is independent of the pumping value and admits a simple explanation (Sec. IV C). We find that this result is relevant because it establishes a simple way for generating squeezed vacua with shapes different from the Gaussian or the TEM_{10} modes. In Sec. V we review the main conclusions of our work.

II. DOPO'S QUANTUM MODEL

We consider a type I DOPO with spherical mirrors pumped by a coherent Gaussian beam of frequency $2\omega_0$, matched to the fundamental transverse mode Ψ_0^0 at that frequency. Within the cavity, pump photons are down converted into signal photons of frequency ω_0 at a $\chi^{(2)}$ crystal that is placed at the cavity waist. The important assumption of this work is that the resonator is tuned, so that ω_0 coincides with the resonance frequency of a unique transverse-mode family f and is detuned far enough from any other family. Within these conditions, the total electric field at the resonator waist plane can be written as

$$\hat{E}(\mathbf{r},t)=\hat{E}_p(\mathbf{r},t)+\hat{E}_s(\mathbf{r},t), \tag{1a}$$

$$\hat{E}_p(\mathbf{r},t)=i\mathcal{F}_p\hat{A}_p(\mathbf{r},t)e^{-2i\omega_0 t}+\text{H.c.}, \tag{1b}$$

$$\hat{E}_s(\mathbf{r},t)=i\mathcal{F}_s\hat{A}_s(\mathbf{r},t)e^{-i\omega_0 t}+\text{H.c.}, \tag{1c}$$

where we have introduced the single-photon field voltages

$$\mathcal{F}_p=\sqrt{2}\mathcal{F}_s=\sqrt{\frac{2\hbar\omega_0}{\varepsilon_0 n_c L_{\text{eff}}}}, \tag{2}$$

where n_c is the crystal refractive index and L_{eff} is the effective resonator length (see Appendix A), and the slowly varying envelopes

$$\hat{A}_p(\mathbf{r},t)=\hat{a}_{00}(t)\Psi_0^0(\mathbf{r}), \tag{3a}$$

$$\hat{A}_s(\mathbf{r},t)=\sum_l \frac{1}{(1+\delta_{0l})}[\hat{a}_{+l}(t)\Psi^{+l}_{(f-l)/2}(\mathbf{r})+\hat{a}_{-l}(t)\Psi^{-l}_{(f-l)/2}(\mathbf{r})], \tag{3b}$$

where the interaction picture boson operators obey the canonical commutation relations $[\hat{a}_m(t),\hat{a}_n^\dagger(t)]=\delta_{mn}$, the Kronecker symbol δ_{0l} is introduced because $\hat{a}_{-0}(t)=\hat{a}_{+0}(t)$, and $\Psi^{\pm l}_{(f-l)/2}(\mathbf{r})$ are the resonator Laguerre-Gauss modes at the resonator waist plane. The expressions for these modes as well as some of their properties are given in Appendix A. Here we just note that

$$\Psi_n^{\pm l}(\mathbf{r})=\mathcal{N}_n^l u_n^l(r)\exp(\pm il\phi), \tag{4}$$

where $\mathbf{r}=(r\cos\phi, r\sin\phi)$ are the resonator waist plane Cartesian coordinates (r and ϕ are the corresponding polar coordinates), $\mathcal{N}_n^l$ is a normalization factor,

$$u_n^l(r)=\frac{1}{w}\left(\frac{\sqrt{2}r}{w}\right)^l L_n^l\left(\frac{2r^2}{w^2}\right)e^{-r^2/w^2}, \tag{5}$$

L_n^l is the modified Laguerre polynomial, and w is the beam waist radius (that depends on frequency). In Eq. (3b) the sum in l runs along all the members of the transverse-mode family f [$l\in\{f,f-2,\ldots,l_0\}$] and this will hold for all sums in l along the rest of the paper. Finally, note that the Laguerre-Gauss modes appearing in Eqs. (3a) and (3b) are evaluated at pump and signal frequencies, respectively, which determine the beam waist radius w (see Appendix A).

For the sake of the latter use we mention here that instead of the Laguerre-Gauss modes one can use the hybrid modes, defined (for $l\neq 0$) as

$$H^l_{\text{c},n}(\mathbf{r})=\frac{1}{\sqrt{2}}[\Psi_n^{+l}(\mathbf{r})+\Psi_n^{-l}(\mathbf{r})]=\sqrt{2}\mathcal{N}_n^l u_n^l(r)\cos(l\phi), \tag{6}$$

$$H^l_{\text{s},n}(\mathbf{r})=\frac{1}{\sqrt{2}i}[\Psi_n^{+l}(\mathbf{r})-\Psi_n^{-l}(\mathbf{r})]=\sqrt{2}\mathcal{N}_n^l u_n^l(r)\sin(l\phi) \tag{7}$$

(see Appendix A) in order to expand the slowly varying envelope of the signal field, whose corresponding boson operators relate to the Laguerre-Gauss mode ones as

$$\hat{a}_{\text{c},l}=[\hat{a}_{+l}(t)+\hat{a}_{-l}(t)]/\sqrt{2}, \tag{8a}$$

$$\hat{a}_{\text{s},l}=i[\hat{a}_{+l}(t)-\hat{a}_{-l}(t)]/\sqrt{2}. \tag{8b}$$

For $l=0$ we still use the Laguerre-Gauss mode $\Psi_n^0(\mathbf{r})$.

In the interaction picture, assuming perfect phase matching as well as exact resonance between the field frequencies and the cavity resonances, the Hamiltonian of the system is $\hat{H}=\hat{H}_{\text{ext}}+\hat{H}_{\text{int}}$ with

$$\hat{H}_{\text{ext}}=i\hbar\mathcal{E}_p(\hat{a}_{00}^\dagger-\hat{a}_{00}), \tag{9a}$$

$$\hat{H}_{\text{int}}=i\hbar\sum_l \frac{\chi_l}{1+\delta_{0l}}(\hat{a}_{00}\hat{a}_{+l}^\dagger\hat{a}_{-l}^\dagger-\hat{a}_{00}^\dagger\hat{a}_{+l}\hat{a}_{-l}), \tag{9b}$$

where $\hat{H}_{\text{ext}}$ describes the external pumping process and $\hat{H}_{\text{int}}$ describes the down-conversion process occurring in the $\chi^{(2)}$ crystal. Notice that OAM conservation imposes the simultaneous creation or annihilation of a pair of signal photons each with an opposite value of l.

The nonlinear coupling constants χ_l in $\hat{H}_{\text{int}}$ read

$$\chi_l = 12\frac{\chi^{(2)} l_c}{w_p}\left(\frac{\omega_0}{n_c L_{\text{eff}}}\right)^{3/2}\sqrt{\frac{\hbar}{\pi\varepsilon_0}}I_l \tag{10}$$

with $\chi^{(2)}$ as the second-order susceptibility of the nonlinear crystal whose thickness is l_c, w_p as the beam spot size at the pump frequency, and

$$I_l = \frac{[(f-l)/2]!}{[(f+l)/2]!}\int_0^{+\infty} du\, e^{-2u}u^l[L^l_{(f-l)/2}(u)]^2, \tag{11}$$

which are proportional to the overlapping integrals between the three modes involved in the particular parametric process. This means that the lower is the OAM of the signal photons, the larger is the nonlinear coupling between these and the pump ones, i.e., $\chi_f < \chi_{f-2} < \cdots < \chi_{l_0}$. This property will play an important role as we show below. Let us finally remark the pump parameter $\mathcal{E}_p$ is proportional to the external pump amplitude and is taken as real without loss of generality.

We will be interested in calculating normally ordered correlations of different mode operators, and to do so we use the generalized P representation and its equivalent set of Langevin equations [15]. In this representation to every pair of boson operators $(\hat{a}_j, \hat{a}_j^\dagger)$ it corresponds a pair of independent stochastic amplitudes (α_j, α_j^+) that are complex conjugated in average, i.e., $\langle\alpha_j^+\rangle = \langle\alpha_j\rangle^*$. The stochastic average of any function of (α_j, α_j^+) equals the corresponding normally ordered quantum-mechanical expected value. The equations of evolution of these amplitudes are derived in Appendix B by following the standard procedure [16,17]. Assuming that losses occur just at one of the cavity mirrors at rates γ_p for the pump mode and γ_s for all possible transverse signal modes (hence the assumption of a large-Fresnel-number resonator), the Langevin equations of the system read

$$\dot{\alpha}_{00} = \mathcal{E}_p - \gamma_p\alpha_{00} - \sum_l \frac{\chi_l}{1+\delta_{0l}}\alpha_{+l}\alpha_{-l}, \tag{12a}$$

$$\dot{\alpha}^+_{00} = \mathcal{E}_p - \gamma_p\alpha^+_{00} - \sum_l \frac{\chi_l}{1+\delta_{0l}}\alpha^+_{+l}\alpha^+_{-l}, \tag{12b}$$

$$\dot{\alpha}_{\pm l} = -\gamma_s\alpha_{\pm l} + \chi_l\alpha^+_{\mp l}\alpha_{00} + \sqrt{\chi_l\alpha_{00}}\xi_{\pm l}(t), \tag{12c}$$

$$\dot{\alpha}^+_{\pm l} = -\gamma_s\alpha^+_{\pm l} + \chi_l\alpha_{\mp l}\alpha^+_{00} + \sqrt{\chi_l\alpha^+_{00}}\xi^+_{\pm l}(t), \tag{12d}$$

where $l \in \{f, f-2, \ldots, l_0\}$. The noises (ξ_l, ξ_l^+) are independent complex Gaussian white noise sources verifying $\langle\xi_l(t)\rangle = \langle\xi_l^+(t)\rangle = 0$ and

$$\langle\xi_l(t)\xi^*_{l'}(t')\rangle = \langle\xi^+_l(t)[\xi^+_{l'}(t')]^*\rangle = \delta_{ll'}\delta(t-t'), \tag{13}$$

being null the rest of correlations. The rest of noises verify $\xi_{-l}(t) = \xi_l^*(t)$ and $\xi^+_{-l}(t) = [\xi^+_l(t)]^*$

Within the generalized P representation, we define the amplitude and phase quadratures, respectively, of a mode j as $X_j = (\alpha_j^+ + \alpha_j)$ and $Y_j = i(\alpha_j^+ - \alpha_j)$. The variance spectrum of quadrature X_j (analogously for Y_j), is measured out of the cavity, and can be calculated as $V^{\text{out}}_{x,j}(\omega) = 1 + S^{\text{out}}_{x,j}(\omega)$ with the squeezing spectrum given, as a function of the intracavity amplitudes, by [4]

$$S^{\text{out}}_{x,j}(\omega) = 2\gamma_j\int_{-\infty}^{+\infty} d\tau\, e^{-i\omega\tau}\langle X_j(t), X_j(t+\tau)\rangle, \tag{14}$$

where the factor $2\gamma_j$ comes from the input-output relations [18]. We use the notation $\langle a, b\rangle = \langle ab\rangle - \langle a\rangle\langle b\rangle$. Notice that $S^{\text{out}}_{x,j}(\omega_s) = -1$ signals perfect squeezing outside the cavity for quadrature X_j at detection frequency ω_s (which must not be confused with the optical frequency, as it has contributions of every pair of modes lying in opposite sidebands around the optical frequency $\omega_j + \omega_s$, where ω_j is the carrier frequency of the detected mode [4]). Hence, by solving the Langevin equations for the amplitudes α_j in terms of the noises ξ_k, one is able to obtain the variances of the quadratures involved in the problem, and thus the squeezing properties of the field.

III. CLASSICAL EMISSION

The classical equations describing the field inside the DOPO are obtained from the quantum Langevin ones by identifying the stochastic amplitudes α_j with the classical normal variables of each mode, by making $\alpha_j^+ \to \alpha_j^*$, and by neglecting noise terms. They read

$$\dot{\alpha}_{00} = \mathcal{E}_p - \gamma_p\alpha_{00} - \sum_l \frac{\chi_l}{1+\delta_{0l}}\alpha_{+l}\alpha_{-l}, \tag{15a}$$

$$\dot{\alpha}_{\pm l} = -\gamma_s\alpha_{\pm l} + \chi_l\alpha^*_{\mp l}\alpha_{00}. \tag{15b}$$

Equation (15) has two types of stationary solutions. If we define the normalized pump parameter as

$$\sigma = \frac{\chi_{l_0}}{\gamma_p\gamma_s}\mathcal{E}_p, \tag{16}$$

it is easy to prove that the below threshold solution

$$\bar{\alpha}_{00} = \mathcal{E}_p/\gamma_p, \quad \bar{\alpha}_l = 0 \quad \forall\, l \tag{17}$$

is stable for $\sigma < 1$ and unstable for $\sigma > 1$ ($\sigma = 1$ thus defines the classical threshold for emission). Apart from this *trivial* solution, there are $(f-l_0)/2+1$ possible stationary solutions in which the signal field is nonzero. The form of these solutions is

$$\bar{\alpha}_{00} = \gamma_s/\chi_k, \quad \bar{\alpha}_{\pm l} = 0 \quad \forall\, l \neq k, \tag{18a}$$

$$\bar{\alpha}_{\pm k} = \rho_k e^{\mp i\theta_k}, \quad \rho_k^2 \equiv \frac{1+\delta_{0,k}}{g^2\kappa_k}\left(\sigma - \frac{1}{\kappa_k}\right) \tag{18b}$$

with

$$g = \frac{\chi_{l_0}}{\sqrt{\gamma_p\gamma_s}}, \quad \kappa_k = \frac{\chi_l\bar{\alpha}_{00}}{\gamma_s} = \frac{\chi_k}{\chi_{l_0}} = \frac{I_k}{I_{l_0}} \tag{19}$$

[see Eqs. (10) and (11)]. Note that in any of these solutions only two opposite OAM values are excited ($\pm k$), the rest remaining below threshold. As for the phases θ_k, $\theta_0 = 0$ and

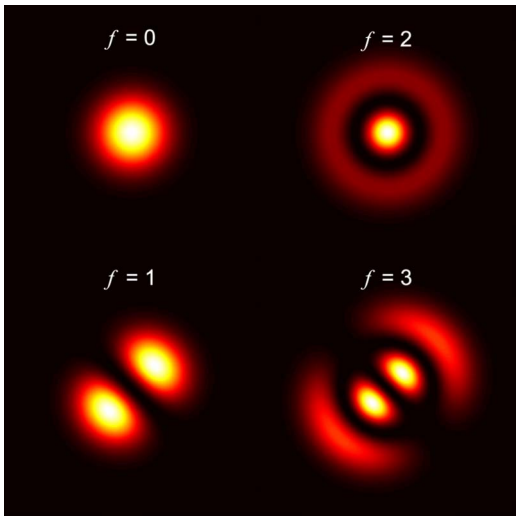

FIG. 1. (Color online) Transverse profile of the signal field modulus above threshold.

$\theta_{k\neq 0}=\theta$ is arbitrary. This arbitrariness appears because Eq. (15) has the symmetry $\alpha_{\pm l}\rightarrow\alpha_{\pm l}\exp(\pm i\beta)$, reflecting the rotational invariance of the system, which leaves undefined the phase difference between opposite OAM modes.

As for the stability, it is easy to show that the only solution that is linearly stable above threshold is precisely that in which the lower OAM modes are switched on, i.e., Eq. (18) for $k=l_0$. These are, in fact, the solutions with the lowest threshold $\sigma=1$ [see Eq. (18)] as $\chi_{l_0}>\chi_l$ as already stressed [see Eq. (10)]. Plugging Eq. (18) into Eq. (3b), one finds the slowly varying amplitudes of these stable classical solutions as

$$\bar{A}_s(\mathbf{r})=\rho_0\Psi^0_{f/2}(\mathbf{r}) \quad \text{for even } f, \tag{20a}$$

$$\bar{A}_s(\mathbf{r})=\sqrt{2}\rho_1 H^1_{\mathrm{c},(f-1)/2}(r,\phi-\theta) \quad \text{for odd } f \tag{20b}$$

with ρ_j given by Eq. (18). In Fig. 1 the square modulus of these slowly varying envelopes are shown for the first four families (note that we have chosen $\theta=\pi/4$ for these figures).

A most important difference occurs between the two cases corresponding to f odd or even. For even f the classical emission $\bar{A}_s(\mathbf{r})$ is rotationally symmetric as $\Psi^0_{f/2}(\mathbf{r})$ is [see Eq. (4)], while for odd f the emitted pattern breaks that symmetry.

IV. SQUEEZING

Now we perform the analysis of quantum fluctuations affecting the classical emission above threshold. First, in order to make the calculations as simple as possible, we consider the limit $\gamma_p\gg\gamma_s$ in which the pump mode can be adiabatically eliminated in Eq. (12) as $\alpha_{00}=\mathcal{E}_p/\gamma_p-\Sigma_l\frac{\chi_l/\gamma_p}{1+\delta_{0l}}\alpha_{+l}\alpha_{-l}$. The resulting equations read

$$\dot{\alpha}_{\pm l}=\gamma_s(-\alpha_{\pm l}+\kappa_l N\alpha^+_{\mp l})+\sqrt{\gamma_s\kappa_l N}\xi_{\pm l}(t), \tag{21a}$$

$$\dot{\alpha}^+_{\pm l}=\gamma_s(-\alpha^+_{\pm l}+\kappa_l N^+\alpha^+_{\mp l})+\sqrt{\gamma_s\kappa_l N^+}\xi^+_{\pm l}(t), \tag{21b}$$

where

$$N=\sigma-g^2\sum_{l'}\frac{\kappa_{l'}}{1+\delta_{0,l'}}\alpha_{+l'}\alpha_{-l'} \tag{22}$$

and N^+ is as N but replacing $\alpha_{l'}$ with $\alpha^+_{l'}$. Moreover, as we will study fluctuations in the linear approximation, the only nonlinearities contained in N that will give a contribution correspond to the classically excited modes ($l'=l_0$) and hence

$$N=\sigma-g^2\frac{\alpha_{+l_0}\alpha_{-l_0}}{1+\delta_{0,l_0}}, \tag{23}$$

which is the expression we will use in the following. We are going to distinguish between the special cases $l=l_0$ on one hand and cases with $l>l_0$, as their properties turn out to be quite different.

A. Special cases $l=l_0$

Here we analyze the squeezing properties of the modes that are classically excited. In this case $\kappa_l=\kappa_{l_0}=1$ [see Eq. (19)] and the Langevin equations (21) and (23) become

(i) case $l_0=0$,

$$\dot{\alpha}_0=\gamma_s(-\alpha_0+N\alpha^+_0)+\sqrt{\gamma_s N}\xi_0(t), \tag{24a}$$

$$N=\sigma-\tfrac{1}{2}g^2\alpha_0\alpha_0, \tag{24b}$$

(ii) case $l_0=1$,

$$\dot{\alpha}_{\pm 1}=\gamma_s(-\alpha_{\pm 1}+N\alpha^+_{\pm 1})+\sqrt{\gamma_s N}\xi_{\pm 1}(t), \tag{25a}$$

$$N=\sigma-g^2\alpha_{+1}\alpha_{-1}. \tag{25b}$$

We note that in neither case the information about the family order f appears (up to here, that information appeared through the reduced coupling parameters κ_l [see Eqs. (10), (11), and (19)]). Moreover, Eq. (24) coincides with those for the paradigmatic single-mode DOPO (see, e.g., [2]), while Eq. (25) does with those for the recently studied DOPO tuned to its first transverse-mode family [13,19]. The conclusions are straightforward:

(1) For any even f ($l_0=0$) the quantum properties of the classically excited mode coincide with those of the usual single-mode DOPO in the linear approximation. At threshold ($\sigma=1$) ideal squeezing is predicted in this approximation and this squeezing degrades as we move apart from threshold. That is why we speak about *critical squeezing* in this case, as the system parameters need to be tuned to a particular value for obtaining the optimum squeezing level. In mathematical terms, this is a consequence of the existence, at the bifurcation point, of a null eigenvalue and of a companion negative eigenvalue that reaches its minimum possible value. The former is the responsible for the "infinite" fluctuations of the amplitude quadrature of the signal mode (which is proportional to the eigenvector associated to the null eigenvalue),

while the latter is the responsible for the complete suppression (in the linear approximation) of the fluctuations in the signal mode phase quadrature. (See below for a more comprehensive explanation.)

(2) For any odd f ($l_0=1$) the quantum properties of the classically excited mode coincide again with those of the single-mode DOPO, i.e., it shows perfect squeezing only when working exactly at the bifurcation. Unlike the previous case the classical emission breaks the rotational invariance of the system and then, apart from the previous critical squeezing property, the system exhibits perfect squeezing in the remaining mode that is spatially crossed with respect to the classically emitted one [13]. As the reason for this lays on the rotational symmetry breaking (and then on OAM conservation [13]), it has nothing to do with bifurcations and the predicted squeezing is *noncritical*. The same squeezing level (perfect, in this case) is obtained at any pumping level. From a mathematical viewpoint one of the eigenvalues governing the stability of the classical solution above threshold is always zero (the eigenvector associated to this eigenvalue is said to be a Goldstone mode), reflecting the indeterminacy of the phase difference between the two signal modes [see Eq. (18)]. This phase difference is nothing but the orientation of the emitted hybrid mode (the TEM_{10} mode in [13]) that results from the coherent superposition of the $\Psi^{+1}_{(f-1)/2}$ and $\Psi^{-1}_{(f-1)/2}$ modes. Thus the physical meaning of the Goldstone mode is that the orientation of the signal mode emitted above threshold by this DOPO diffuses with time and is thus undetermined. This eigenvalue is accompanied by another eigenvalue, which always takes its minimum possible value, with the consequence that the amplitude of its associated eigenvector has no fluctuations at all. This last eigenvector can be easily identified with the OAM of the emitted pattern, which is nothing but another hybrid mode spatially crossed (orthogonal) with respect to the bright one. This shows that the generation of noncritical squeezing through the spontaneous rotational symmetry breaking mechanism is not particular of the model considered in [13], but should be a general phenomenon. We address the reader to [13] for full details of this phenomenon.

B. Cases $l>l_0$: Squeezing of higher OAM modes

In this case the amplitudes α_l and α_l^+ are very small (they are null in the classical limit even if the system is above threshold) and then, in the linear approximation, we are considering that the nonlinear function N (23) appearing in Eq. (21) must be evaluated at its classical value (18) as not doing would introduce higher-order corrections that must be neglected in the used linear approximation. One then obtains $N=1$ and the Langevin equations become

$$\dot{\alpha}_{\pm l} = \gamma_s(-\alpha_{\pm l} + \kappa_l \alpha^+_{\mp l}) + \sqrt{\gamma_s \kappa_l}\xi_{\pm l}(t), \tag{26a}$$

$$\dot{\alpha}^+_{\pm l} = \gamma_s(-\alpha^+_{\pm l} + \kappa_l \alpha^+_{\mp l}) + \sqrt{\gamma_s \kappa_l}\xi^+_{\pm l}(t). \tag{26b}$$

As is evident, the evolution of the different pairs of OAM $\pm l$ is decoupled, which allows us to analyze separately the quantum properties of each l couple. Moreover, the evolution of these fluctuations does not depend on whether the family is odd or even.

The study of Eq. (26) is facilitated by expressing it in vector form as

$$\dot{\mathbf{a}}_l = \mathcal{L}_l \mathbf{a}_l + \sqrt{\gamma_s \kappa_l}\boldsymbol{\xi}_l(t) \tag{27}$$

with

$$\mathbf{a}_l = \mathrm{col}(\alpha_{+l}, \alpha^+_{+l}, \alpha_{-l}, \alpha^+_{-l}), \tag{28a}$$

$$\boldsymbol{\xi}_l = \mathrm{col}(\xi_l(t), \xi^+_l(t), \xi^*_l(t), [\xi^+_l(t)]^*), \tag{28b}$$

$$\mathcal{L}_l = \gamma_s \begin{pmatrix} -1 & 0 & 0 & \kappa_l \\ 0 & -1 & \kappa_l & 0 \\ 0 & \kappa_l & -1 & 0 \\ \kappa_l & 0 & 0 & -1 \end{pmatrix}, \tag{28c}$$

where we remind that $0<\kappa_l<1$ [see Eq. (19)]. Linear matrix $\mathcal{L}_l$ has eigenvalues $\lambda^l_1=\lambda^l_2=-\gamma_s(1-\kappa_l)$ and $\lambda^l_3=\lambda^l_4=-\gamma_s(1+\kappa_l)$ with corresponding eigenvectors [20]

$$\mathbf{w}^l_{1,2} = \tfrac{1}{2}\mathrm{col}(1, \pm 1, \pm 1, 1), \tag{29a}$$

$$\mathbf{w}^l_{3,4} = \tfrac{1}{2}\mathrm{col}(1, \pm 1, \mp 1, -1). \tag{29b}$$

By projecting the linear Langevin system (27) onto $\mathbf{w}^l_j$, we find

$$\dot{c}^l_{1,4} = -\gamma_s(1 \mp \kappa_l)c^l_1 + \sqrt{\gamma_s \kappa_l}\eta^l_{1,4}(t), \tag{30a}$$

$$\dot{c}^l_{2,3} = -\gamma_s(1 \mp \kappa_l)c^l_3 + i\sqrt{\gamma_s \kappa_l}\eta^l_{2,3}(t), \tag{30b}$$

where we defined the projections

$$c^l_j(t) = \mathbf{w}^l_j \cdot \mathbf{a}_l(t), \tag{31}$$

and the four other real noises

$$\eta^l_{1,4}(t) = \mathbf{w}^l_{1,4} \cdot \xi_l(t) = \mathrm{Re}[\xi_l(t) \pm \xi^+_l(t)], \tag{32a}$$

$$\eta^l_{2,3}(t) = -i\mathbf{w}^l_{2,3} \cdot \xi_l(t) = \mathrm{Im}[\xi_l(t) \mp \xi^+_l(t)], \tag{32b}$$

which satisfy the statistical properties

$$\langle \eta^l_j(t) \rangle = 0, \quad \langle \eta^l_m(t_1)\eta^l_n(t_2) \rangle = \delta_{mn}\delta(t_1 - t_2). \tag{33}$$

Equation (30) is solved with standard methods. The variance spectra for projections c_j, defined as

$$\tilde{C}_j(\omega) = \int_{-\infty}^{+\infty} d\tau\, e^{-i\omega\tau}\langle c_j(t), c_j(t+\tau)\rangle, \tag{34}$$

read, in the stationary limit $t \gg \lambda_j^{-1}$,

$$\tilde{C}^l_{1,3}(\omega) = -\tilde{C}^l_{2,4}(\omega) = \pm \frac{\gamma_s \kappa_l}{[\gamma_s(1 \mp \kappa_l)]^2 + \omega^2}. \tag{35}$$

The advantage of the eigensystem method we are using [10,11,13] is that the relevant quadratures of the problem appear in a natural way, as the projections c^l_j are related to the problem quadratures through

$$X_{c,l} = \sqrt{2}c^l_1, \quad X_{s,l} = i\sqrt{2}c^l_2, \tag{36a}$$

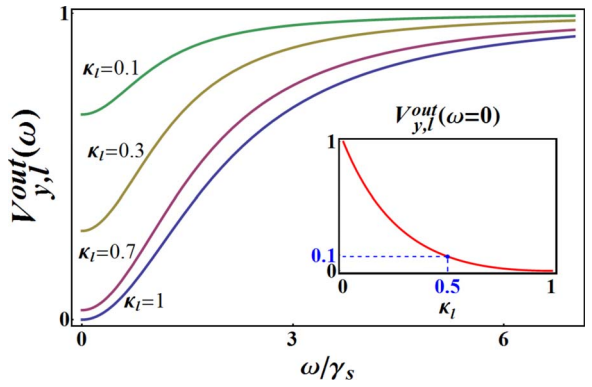

FIG. 2. (Color online) Variance spectra of the phase quadratures of some hybrid modes with $l \neq l_0$. The inset shows the same quantity at $\omega=0$ as a function of κ_l.

$$Y_{c,l} = -i\sqrt{2}c_4^l, \quad Y_{s,l} = \sqrt{2}c_3^l, \tag{36b}$$

where

$$X_{j,l} = (\alpha_{j,l}^+ + \alpha_{j,l}), \tag{37}$$

$$Y_{j,l} = i(\alpha_{j,l}^+ + \alpha_{j,l}) \tag{38}$$

refer to the hybrid mode $H^l_{j,(f-l)/2}(\mathbf{r})$ as it can be easily seen from Eq. (8). These simple relations are the consequence of the appropriate choice of the eigenvectors of $\mathcal{L}_l$ [20].

We are now in conditions to find out the squeezing spectra of the quadratures. By using Eq. (14) together with the relations above, we get $S^{out}_{x,c,l}(\omega)=S^{out}_{x,s,l}(\omega)=4\gamma_s\tilde{C}^l_1(\omega)$ and $S^{out}_{y,c,l}(\omega)=S^{out}_{y,s,l}(\omega)=4\gamma_s\tilde{C}^l_3(\omega)$, i.e., the squeezing of the phase quadratures is

$$S^{out}_{y,j,l}(\omega) = -\frac{4\kappa_l}{(1+\kappa_l)^2+(\omega/\gamma_s)^2}, \quad j=c,s. \tag{39}$$

This expression clearly shows that the phase quadratures $Y_{j,l}$ $(j=c,s)$ of both $H^l_{c,(f-l)/2}(\mathbf{r})$ and $H^l_{s,(f-l)/2}(\mathbf{r})$ hybrid modes (i) have the same fluctuations properties, (ii) are noncritically squeezed as $S^{out}_{y,j,l}(\omega)<0$ at any noise frequency ω and this value is independent of the distance from threshold [it is however dependent on the OAM value through the value of the ratio κ_l (19)], (iii) and exhibit maximum squeezing at $\omega=0$. This is the main result of our paper and we pass to discuss it.

TABLE I. Percentage of noise reduction for the nonamplified hybrid modes $l \neq l_0$ lying in even families. Note that large levels of squeezing are obtained for the lower angular momentum modes.

$f\backslash l$	2	4	6	8	10	12
2	88.9					
4	96.0	49.0				
6	98.0	71.0	18.1			
8	98.8	81.6	36.8	5.6		
10	99.2	87.4	51.4	14.7	1.6	
12	99.4	90.9	62.1	24.9	5.1	0.4

TABLE II. Same as Table I, but for odd families. Large levels of squeezing are also obtained in this case for the lower angular momentum modes.

$f\backslash l$	3	5	7	9	11	13
3	75.0					
5	88.9	33.1				
7	93.8	55.6	10.8			
9	96.0	69.1	24.9	3.1		
11	97.2	77.6	38.0	9.1	0.9	
13	98.0	83.0	49.0	16.6	3.0	0.2

C. Discussion

We have shown that the light emitted by a DOPO with a large-Fresnel-number cavity with spherical mirrors exhibits a variety of squeezing properties. On one hand there is the usual critical squeezing appearing at the oscillation threshold [2] associated with the classically emitted solution. There is also the noncritical squeezing due to the spontaneous breaking of the rotational symmetry that appears above threshold for odd f $(l_0=1)$ [13]. Also a type of squeezing behavior has been derived for all hybrid modes with $l>l_0$, which remain off at the classical level once the oscillation threshold is crossed, consisting in that their phase quadratures are noncritically squeezed for any l, as shown by Eq. (39).

The variance spectrum for either of the phase quadratures $V^{out}_{y,l}(\omega)=1+S^{out}_{y,j,l}(\omega)$ for $j=c$ or $j=s$ is represented in Fig. 2 for different values of κ_l [see Eq. (19)]. In the figure, $V^{out}_{y,l}(\omega=0)$ is also shown, at the inset, as a function of κ_l. Clearly, as $\kappa_l=\chi_l/\chi_{l_0}\to 1$, which occurs as $l\to l_0$, nearly perfect squeezing is found at $\omega=0$. Notice that more than 90% of squeezing can be achieved if $\kappa_l>0.5$. But the ratio $\kappa_l=I_l/I_{l_0}$, which is obtained from Eq. (10), is solely determined by geometrical reasons, and thus the squeezing properties of these higher OAM modes do not depend on the system parameters (of course we must remind that we assumed equal cavity losses for all modes).

In order to better appreciate the large amounts of squeezing exhibited by these modes, we give their associated noise reduction in percentage for different even (odd) families in Table I (Table II). Notice that the largest squeezing occurs for large values of f and small values of l and works better for even families.

It is to be remarked that both the hybrid mode $H^l_{c,n}(\mathbf{r})$ and its orthogonal $H^l_{s,n}(\mathbf{r})$ have the same squeezing properties. This means that the orientation of the mode is irrelevant, as a hybrid mode rotated an arbitrary angle β with respect to the x axis, which is given by

$$H^l_{\beta,n}(\mathbf{r}) = H^l_{c,n}(r,\phi-\beta) = H^l_{c,n}(\mathbf{r})\cos(l\beta) + H^l_{s,n}(\mathbf{r})\sin(l\beta), \tag{40}$$

also has the same squeezing properties. This is in clear con-

trast to the perfectly squeezed mode in the $l=l_0=1$ case [13], which has not an arbitrary orientation but is orthogonal to the classically excited mode at every instance. Of course, the reason is that the modes analyzed here are below their threshold, at difference with the case in [13].

So far we have proven that the higher OAM modes show noise reduction in their phase quadrature. Let us see why is this occurring. The coefficient that rules the squeezing properties of the $l \neq l_0$ modes is κ_l [see Eq. (39)]. Both above and below threshold, κ_l can be written in terms of the stationary pump field as $\kappa_l = \chi_l \bar{\alpha}_{00} / \gamma_s$ [see Eq. (19)]. Below threshold $\bar{\alpha}_{00}$ increases linearly with the external pump amplitude [see Eq. (17)] and hence so does κ_l. But once the bifurcation is reached and the DOPO starts emitting the l_0 mode(s), the value of $\bar{\alpha}_{00}$ saturates and remains constant irrespective of the pump value [see Eq. (18)] leading to $\kappa_l = I_l / I_{l_0}$ above threshold, which is independent of the pump value. This implies that the value of κ_l will remain fixed to that at the bifurcation once the DOPO is above threshold and, consequently, the squeezing level of these modes becomes noncritical.

V. CONCLUSIONS

We have shown that tuning large-Fresnel-number DOPOs with spherical mirrors to transverse families is a simple way for generating squeezed light with the shape of hybrid Laguerre-Gauss modes with OAM $l > l_0$ with $l_0=0$ or 1 depending on the even or odd character of the selected transverse-mode family. The behavior of the system can be resumed as follows. Above threshold, only the hybrid mode with $l=l_0$ is amplified and the rest of modes (those with $l > l_0$) remain off. The amplified modes exhibit squeezing properties that can be found in the literature (see [2] for $l_0=0$ and [13] for $l_0=1$) as shown in Sec. IV A.

The surprising result is that hybrid modes with $l > l_0$ exhibit a large degree of squeezing together with the fact that this squeezing is noncritical, i.e., it remains fixed irrespective of the pump level when the system is above threshold. Thus, squeezed vacua with the shape of higher-order hybrid modes can be generated by normal DOPOs if these have a large Fresnel number.

In our model we assumed equal cavity losses for all signal modes (in fact, equal cavity losses for all signal modes belonging to the same family; this is the precise meaning we give to the expression large-Fresnel-number cavity). As we have explained, the squeezing level of modes with OAM $l > l_0$ depends on the distance between their threshold and that for the mode(s) with lowest OAM l_0. Hence, differences in the values of their decay rates could modify quantitatively the results we have presented, as this would change the threshold for the different modes. If fact, if tailoring the cavity losses for the different modes would be possible, one could obtain even smaller quantum fluctuations for these empty modes if their corresponding thresholds were made closer to that of the l_0 mode. We also assumed perfect cavity resonance for a particular family of modes. We do not expect that detuning changes our main conclusions, as detuning affects equally all modes within the same family (apart, of course, from the fact that if the detuning is half the value the transverse free spectral range, competition phenomena between the involved families will manifest, something that is not considered in our model). Adding detuning would have the same consequences as in the single-mode DOPO: it will increase the threshold and change the phase of the amplified mode (and hence of the squeezed quadratures).

We finally note that Laguerre-Gauss modes are becoming important for several purposes, e.g., in quantum information processing and in manipulation of atoms [8] just to mention a couple. We hope that our results can be of relevance as squeezed hybrid modes or, equivalently, entangled Laguerre-Gauss modes, can be of utility for these purposes.

ACKNOWLEDGMENTS

This work was supported by the Spanish Ministerio de Eduación y Ciencia and the European Union FEDER through Project No. FIS2005-07931-C03-01 and FIS2008-06024-C03-01. C.N.B. is a grant holder of the FPU program of the Ministerio de Educación y Ciencia (Spain).

APPENDIX A: CAVITY MODES

For the sake of clarity, we find it convenient to review the main properties of the cavity modes in a Fabry-Perot resonator with spherical mirrors (see, e.g., [21] for more details). Within the paraxial approximation, it is well known that the Laguerre-Gauss modes form a complete set of spatial modes describing the light inside the resonator. Let R_1 and R_2 denote the curvature radius of the cavity mirrors and $L_{\text{eff}}=L-(1-1/n_c)l_c$ denotes the effective cavity length with L as the geometrical length of the resonator and l_c and n_c as the length and refractive index, respectively, of the $\chi^{(2)}$ crystal. Then the Laguerre-Gauss modes at the resonator waist plane can be written as

$$\Psi_n^{\pm l}(\mathbf{r}) = \mathcal{N}_n^l u_n^l(r) \exp(\pm i l \phi) \tag{A1}$$

with $\mathbf{r}=(x,y)$ as the transverse coordinates where $\mathbf{r}=r(\cos\phi, \sin\phi)$ is its polar decomposition, $\mathcal{N}_n^l$ is a normalization factor, and

$$u_n^l(r) = \frac{1}{w}\left(\frac{\sqrt{2}r}{w}\right)^l L_n^l\left(\frac{2r^2}{w^2}\right) e^{-r^2/w^2}, \tag{A2}$$

where L_n^l is the modified Laguerre polynomial with radial and polar indices $n, l \in \mathbb{N}$, which are given by the Rodrigues formula

$$L_n^l(v) = \frac{1}{n!} e^v \frac{1}{v^l} \frac{d^n}{dv^n}(e^{-v} v^l v^n). \tag{A3}$$

By choosing the normalization factor as

$$\mathcal{N}_n^l = \sqrt{\frac{2}{\pi}\frac{n!}{(n+l)!}}, \tag{A4}$$

the following orthogonality relation holds:

$$\int_0^{2\pi} d\phi \int_0^{\infty} r dr [\Psi_n^{\pm l}(\mathbf{r})]^* \Psi_{n'}^{\pm l'}(\mathbf{r}) = \delta_{ll'}\delta_{nn'}. \tag{A5}$$

The beam spot size at the cavity waist, w, is given by

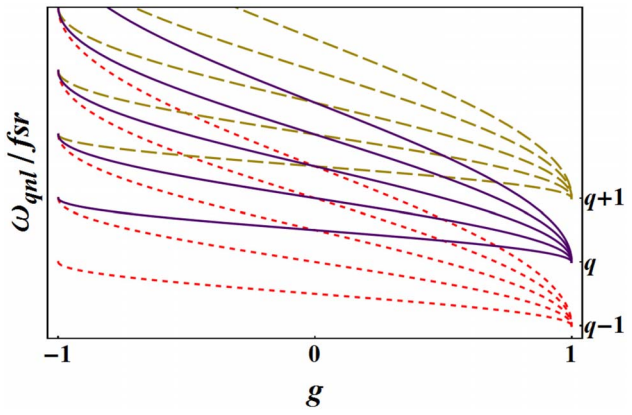

FIG. 3. (Color online) Resonance frequencies of the first four families corresponding to three consecutive longitudinal modes, as a function of the g parameter of a symmetrical resonator. Different families corresponding to the same longitudinal mode have the same color and dashing. The family order f increases with the frequency.

$$w^2 = \frac{2cL_{\text{eff}}}{\omega}\frac{\sqrt{g_1g_2(1-g_1g_2)}}{g_1+g_2-2g_1g_2} \tag{A6}$$

with $g_j=1-L_{\text{eff}}/R_j$ and ω as the beam frequency.

The Laguerre-Gauss basis is recommended in order to visualize the OAM of the field, as these modes are eigenstates of the OAM operator $-i\partial_\phi$ with eigenvalues $\pm l$. Concerning the resonance frequency of the different $\Psi_n^{\pm l}$ modes, they are different in general for each mode. Concretely $\omega_{qnl}=q\pi c/L_{\text{eff}}+\Delta\omega_{nl}$ with q as an integer (different q's correspond to different longitudinal cavity modes) and the transverse part of the resonance frequency is given by

$$\Delta\omega_{nl} = \frac{c}{L_{\text{eff}}}(1+2n+l)\arccos(\sqrt{g_1g_2}). \tag{A7}$$

Hence, cavity modes having the same *family order* $f=(2n+l)$ have the same frequency and are said to be members of the same family f. It is clear that family f consists of the set of $f+1$ Laguerre-Gauss modes $\{\Psi^{\pm l}_{(f-l)/2}\}$ with $l=f,f-2,\ldots,l_0$, having OAM $\pm f,\pm(f-2),\ldots,\pm l_0$, respectively. The lower OAM modes have $l_0=0$ or 1 for even or odd f, respectively. In Fig. 3 we represent ω_{qnl} (in units of the free spectral range, $fsr=\pi c/L_{\text{eff}}$) for several modes as a function of g for *symmetric* resonators (those for which $g_1=g_2\equiv g$) which are *stable* (i.e., $-1<g<1$; be reminded that $g=1$ corresponds to a planar mirrors resonator, $g=0$ to a confocal resonator, and $g=-1$ to a concentric resonator). It can be clearly appreciated that different transverse families corresponding to different longitudinal modes can have the same frequency for rational values of $(\arccos g)/\pi$. Below we assume that different families have different frequencies, i.e., that this quantity has an irrational value.

APPENDIX B: LANGEVIN EQUATIONS

Next we outline the derivation of the Langevin equations (12). Neglecting the effect of thermal photons, the master equation ruling the evolution of the system density operator [16] reads

$$\frac{\partial}{\partial t}\hat{\varrho} = \frac{1}{i\hbar}[\hat{H},\hat{\varrho}] + \sum_{\pm l}\gamma_s(2\hat{a}_l\hat{\varrho}\hat{a}_l^\dagger - \hat{a}_l^\dagger\hat{a}_l\hat{\varrho} - \hat{\varrho}\hat{a}_l^\dagger\hat{a}_l) + \gamma_p(2\hat{a}_{00}\hat{\varrho}\hat{a}_{00}^\dagger - \hat{a}_{00}^\dagger\hat{a}_{00}\hat{\varrho} - \hat{\varrho}\hat{a}_{00}^\dagger\hat{a}_{00}), \tag{B1}$$

where losses are assumed to occur in only one of the cavity mirrors and $\hat{H}$ is given by Eq. (9). Now we use the positive P representation [15,17] of the density operator, which allows the evaluation of expected values of normally ordered operators as averages of functions in phase space. By using standard methods [15,17], the master equation (B1) is then transformed into a Fokker-Planck-type equation for $P(\boldsymbol{\alpha},\boldsymbol{\alpha}^+)$, where all the coherent amplitudes are collected into the vector

$$\boldsymbol{\alpha} = \text{col}(\alpha_{00},\alpha_{00}^+,\alpha_{+l},\alpha_{+l}^+,\alpha_{-l},\alpha_{-l}^+). \tag{B2}$$

The equation for P reads

$$\frac{\partial}{\partial t}P = \left[-\sum_i\frac{\partial}{\partial\alpha_i}A_i + \frac{1}{2}\sum_{i,j}\frac{\partial^2}{\partial\alpha_i\,\partial\,\alpha_j}\mathcal{D}_{ij}\right]P, \tag{B3}$$

where α_i means the ith element of $\boldsymbol{\alpha}$ with

$$A_1 = \mathcal{E}_p - \gamma_p\alpha_{00} - \sum_l\frac{\chi_l}{1+\delta_{0l}}\alpha_{-l}\alpha_{+l}, \tag{B4}$$

$$A_3 = -\gamma_s\alpha_{+l} + \chi_l\alpha_{00}\alpha_{+l}^+, \tag{B5}$$

$$A_5 = -\gamma_s\alpha_{-l} + \chi_l\alpha_{00}\alpha_{-l}^+, \tag{B6}$$

$$\mathcal{D}_{35} = \mathcal{D}_{53} = \chi_l\alpha_{00}, \quad \mathcal{D}_{46} = \mathcal{D}_{64} = \chi_l\alpha_{00}^+, \tag{B7}$$

and $A_{2,4,6}$ are obtained from $A_{1,3,5}$ by changing $\alpha_j\leftrightarrow\alpha_j^+$. Any other element of the diffusion matrix $\mathcal{D}$ is null.

Next, as stated by the Itô theorem [22], this Fokker-Planck equation is mapped onto the set of coupled stochastic (Langevin) equations,

$$\dot{\boldsymbol{\alpha}} = \mathbf{A}(\boldsymbol{\alpha}) + \mathcal{B}(\boldsymbol{\alpha})\cdot\boldsymbol{\eta}(t), \tag{B8}$$

where $\boldsymbol{\eta}$ is a vector with real white noises as components, each of them satisfying the statistical properties defined in Eq. (33), $\mathbf{A}$ is a vector with components A_i $(i=1,6)$ defined above, and the *noise matrix* $\mathcal{B}$ is defined by $\mathcal{D}=\mathcal{B}\cdot\mathcal{B}^T$. The equivalence between the Fokker-Planck equation and the Langevin system has to be understood as $\langle f(\boldsymbol{\alpha})\rangle_P = \langle f(\boldsymbol{\alpha})\rangle_{\text{stochastic}}$, i.e., phase space averages are equal to averages made by using the statistical properties of the noise vector $\boldsymbol{\eta}(t)$.

As for the diffusion matrix $\mathcal{D}$, it is composed of uncoupled minors for each one of the $\pm l$ and 00 subspaces, and then so does matrix $\mathcal{B}$. In addition, the noise matrix minor associated to the pump mode is the zero matrix as this is its associated minor in $\mathcal{D}$. One possible choice for the minors associated to $\pm l$ modes is

$$\mathcal{B}_l = \sqrt{\frac{\chi_l}{2}} \begin{pmatrix} \sqrt{\alpha_{00}} & 0 & i\sqrt{\alpha_{00}} & 0 \\ 0 & \sqrt{\alpha_{00}^+} & 0 & i\sqrt{\alpha_{00}^+} \\ \sqrt{\alpha_{00}} & 0 & -i\sqrt{\alpha_{00}} & 0 \\ 0 & \sqrt{\alpha_{00}^+} & 0 & -i\sqrt{\alpha_{00}^+} \end{pmatrix} \tag{B9}$$

for $l \neq 0$ and

$$\mathcal{B}_0 = \sqrt{\chi_0} \begin{pmatrix} \sqrt{\alpha_{00}} & 0 \\ 0 & \sqrt{\alpha_{00}^+} \end{pmatrix} \tag{B10}$$

for $l=0$. Finally, inserting this noise matrix into the equivalent Langevin system (B8), we get Eq. (12).

[1] R. Loudon and P. L. Knight, J. Mod. Opt. **34**, 709 (1987).

[2] D. F. Walls and G. J. Milburn, *Quantum Optics* (Springer, New York, 1994).

[3] *Quantum Squeezing*, edited by P. D. Drummond and Z. Ficek (Springer, New York, 2004).

[4] J. Gea-Banacloche, N. Lu, L. M. Pedrotti, S. Prasad, M. O. Scully, and K. Wodkiewicz, Phys. Rev. A **41**, 369 (1990).

[5] H. Vahlbruch, M. Mehmet, S. Chelkowski, B. Hage, A. Franzen, N. Lastzka, S. Goszler, K. Danzmann, and R. Schnabel, Phys. Rev. Lett. **100**, 033602 (2008); see also Y. Takeno, M. Yukawa, H. Yonezawa and A. Furusawa, Opt. Express **15**, 4321 (2007).

[6] S. L. Braunstein and P. van Loock, Rev. Mod. Phys. **77**, 513 (2005).

[7] C. Fabre, J. B. Fouet, and A. Mâitre, Opt. Lett. **25**, 76 (2000); N. Treps, U. Andersen, B. Buchler, P. K. Lam, A. Mâitre, H. A. Bachor, and C. Fabre, Phys. Rev. Lett. **88**, 203601 (2002); N. Treps, N. Grosse, W. P. Bowen, C. Fabre, H. -A. Bachor, and P. K. Lam, Science **301**, 940 (2003).

[8] See, e.g., S. Franke-Arnold and A. S. Arnold, Am. Sci. **96**, 226 (2008).

[9] A. Gatti and L. A. Lugiato, Phys. Rev. A **52**, 1675 (1995).

[10] I. Pérez-Arjona, E. Roldán, and G. J. de Valcárcel, Europhys. Lett. **74**, 247 (2006).

[11] I. Pérez-Arjona, E. Roldán, and G. J. de Valcárcel, Phys. Rev. A **75**, 063802 (2007).

[12] K. I. Petsas, A. Gatti, and L. A. Lugiato, Quantum Semiclassic. Opt. **10**, 789 (1998).

[13] C. Navarrete-Benlloch, E. Roldán, and G. J. de Valcárcel, Phys. Rev. Lett. **100**, 203601 (2008).

[14] Related experiments have been started for the simplest case ($f=1$) we treated in [13]; see M. Lassen, G. Leuchs, and U. L. Anderson, e-print arXiv:0901.2783.

[15] P. D. Drummond and C. W. Gardiner, J. Phys. A **13**, 2353 (1980).

[16] H. J. Carmichael, *Statistical Methods in Quantum Optics 1* (Springer, New York, 1999).

[17] C. W. Gardiner and P. Zoller, *Quantum Noise* (Springer, New York, 2000).

[18] M. J. Collett and C. W. Gardiner, Phys. Rev. A **30**, 1386 (1984).

[19] Note that $\chi\alpha_0$ in [13] reads $\gamma_s N$ in our notation.

[20] It is worth remarking one point on the diagonalization of operator $\mathcal{L}_l$. Its eigensystem consists of two degenerate subspaces. How must the two eigenvectors expanding each degenerate subspace be chosen? As will become clearer later, the more appropriate choice is the one that makes the operators related to the projections c_j be either Hermitian or anti-Hermitian, so that they coincide (up to a real or imaginary constant) with some observables of interest. For example, with our choice of eigenvectors we see that the operators related to c_1^l and c_2^l are $\hat{c}_{1,2}^l = \hat{a}_{+l} \pm \hat{a}_{+l}^\dagger \pm \hat{a}_{-l} + \hat{a}_{-l}^\dagger$ [see Eq. (29)], which are Hermitian and anti-Hermitian, respectively.

[21] N. Hodgson and H. Weber, *Laser Resonators and Beam Propagation* (Springer, New York, 2005).

[22] L. Arnold, *Stochastic Differential Equations: Theory and Applications* (Wiley, New York, 1974).